Barrett's neoplasia may be difficult to locate. We consider that an investigation focusing only on Barrett's neoplasia in the upper esophagus (for example, 5-10 cm above the lower esophageal sphincter) would be quite interesting and may reveal important information about the endoscopic surveillance of LSBE cases. If an asymmetrical distribution of Barrett's esophagus is found even in the upper portion of the esophagus, it may be caused not by an uneven reflux of gastric acid but rather by different mechanisms such as uneven flow of swallowed saliva and uneven chemical clearance in the esophagus.

We applaud the effort of Cassani et al, who have provided an extension of previous observations of the distal esophagus to the middle part of the esophagus.

DISCLOSURE

All authors disclosed no financial relationships relevant to this publication.

Norihisa Ishimura, MD
Shunji Ishihara, MD
Yoshikazu Kinoshita, MD
Department of Gastroenterology and Hepatology
Shimane University School of Medicine
Izumo, Shimane, Japan

REFERENCES

1. Cassani L, Sumner E, Slaughter JC, et al. Directional distribution of neoplasia in Barrett's esophagus is not influenced by distance from the gastroesophageal junction. Gastrointest Endosc 2013;77:877-82.
2. Katsube T, Adachi K, Furuta K, et al. Difference in localization of esophageal mucosal breaks among grades of esophagitis. J Gastroenterol Hepatol 2006;21:1656-9.
3. Edebo A, Vieth M, Tam W, et al. Circumferential and axial distribution of esophageal mucosal damage in reflux disease. Dis Esophagus 2007;20:232-8.
4. Okita K, Amano Y, Takahashi Y, et al. Barrett's esophagus in Japanese patients: its prevalence, form, and elongation. J Gastroenterol 2008;43:928-34.
5. Moriyama N, Amano Y, Okita K, et al. Localization of early-stage dysplastic Barrett's lesions in patients with short-segment Barrett's esophagus. Am J Gastroenterol 2006;101:2666-7.
6. Pech O, Gossner L, Manner H, et al. Prospective evaluation of the macroscopic types and location of early Barrett's neoplasia in 380 lesions. Endoscopy 2007;39:588-93.
7. Okamoto E, Amano Y, Fukuhara H, et al. Does gastroesophageal reflux have an influence on bleeding from esophageal varices? J Gastroenterol 2008;43:803-8.
8. Kinoshita Y, Furuta K, Adachi K, et al. Asymmetrical circumferential distribution of esophagogastric junctional lesions: anatomical and physiological considerations. J Gastroenterol 2009;44:812-8.
9. Ohara S, Furuta K, Adachi K, et al. Radially asymmetric gastroesophageal acid reflux in the distal esophagus: examinations with novel pH sensor catheter equipped with 8 pH sensors. J Gastroenterol 2012;47:1221-7.

http://dx.doi.org/10.1016/j.gie.2013.08.004

Response:

We thank Drs Ishimura, Ishihara, and Kinoshita for their insightful comments on our study of directional preference of Barrett's associated neoplasia.

Our study identified a directional preference of Barrett's associated neoplasia for lesions within 3 cm of the gastroesophageal junction. This corroborates data from studies cited in our article, as well as work described by Ishimura and colleagues, and additionally a study in press by Enestvedt and colleagues.[1] Although we do not have direct measures of esophageal acid exposure from the study participants in our cohort, we agree that an asymmetric distribution of acid-related injury in the distal esophagus is a likely underlying mechanism for this directional preference of neoplasia.

The novel finding in our study was that the preference for the right hemisphere (1 to 5 o'clock in our analysis) persisted even for lesions detected 3 cm or more above the gastroesophageal junction. Our initial hypothesis was that the distribution of lesions would become more random with increasing distance from the gastroesophageal junction. We agree, as suggested by Drs Ishimura, Ishihara, and Kinoshita, that the contribution of factors other than reflux, such as salivary exposure or esophageal clearance, may merit further investigation.

Future studies will be needed to validate our findings and should include attention to minimizing the potential for a "gaze preference" for the right hemisphere, resulting in detection bias. In the meantime, we suggest close inspection of the 1 o'clock to 5 o'clock locations of the esophagus in both short-segment and long-segment Barrett's esophagus for the optimal detection of neoplasia.

DISCLOSURE

All authors disclosed no financial relationships relevant to this publication.

Lisa Cassani, MD
Patrick Yachimski, MD, MPH
Division of Gastroenterology, Hepatology & Nutrition
Vanderbilt University Medical Center
Nashville, Tennessee, USA

REFERENCE

1. Enestvedt BK, Lugo R, Guarner-Argente C, et al. Location, location, location: does early cancer in Barrett's esophagus have a preference? Gastrointest Endosc 2013;78:462-7.

http://dx.doi.org/10.1016/j.gie.2013.08.025

J Gastroenterol (2014) 49:1307–1313
DOI 10.1007/s00535-013-0876-0

The Japanese Society of Gastroenterology

ORIGINAL ARTICLE—ALIMENTARY TRACT

Effects of mosapride on esophageal motor activity and esophagogastric junction compliance in healthy volunteers

Kousuke Fukazawa · Kenji Furuta · Kyoichi Adachi · Yoshiya Moritou · Tsukasa Saito · Ryusaku Kusunoki · Goichi Uno · Shino Shimura · Masahito Aimi · Shunji Ohara · Shunji Ishihara · Yoshikazu Kinoshita

Received: 24 June 2013 / Accepted: 20 August 2013 / Published online: 7 September 2013

Abstract
Background The effects of the prokinetic drug mosapride on esophageal motor activity vary at standard doses. In addition to esophageal motor activities, compliance of the esophagogastric junction (EGJ) is important for prevention of gastroesophageal reflux. However, the effects of mosapride on EGJ compliance have not been reported. Here, we investigated the effects of high-dose mosapride on esophageal motor activities and EGJ compliance.
Methods Nine healthy volunteers were enrolled in the study. Peristaltic esophageal contraction and lower esophageal sphincter pressures before and after administration of 40 mg mosapride were examined by high resolution esophageal manometry. Esophageal compliance was also investigated by intra-esophageal impedance planimetry (EndoFLIP®).
Results High-dose mosapride augmented peristaltic contractions, especially in the distal esophageal segments ($P < 0.05$). The mean resting lower esophageal sphincter pressure was elevated from 25.0 mmHg before administration to 28.9 mmHg after ($P < 0.05$). In addition, mosapride significantly reduced EGJ compliance ($P < 0.05$).
Conclusions Mosapride at 40 mg augmented esophageal motor activities and reduced EGJ compliance in healthy volunteers.

Keywords Compliance · Esophagogastric junction · Manometry · Mosapride

K. Fukazawa (✉) · K. Furuta · Y. Moritou · T. Saito · R. Kusunoki · G. Uno · S. Shimura · M. Aimi · S. Ohara · S. Ishihara · Y. Kinoshita
Second Department of Internal Medicine, Shimane University Faculty of Medicine, 89-1 Enya-cho, Izumo, Shimane 693-8501, Japan
e-mail: fkousuke@waltz.ocn.ne.jp

M. Aimi
e-mail: aimi@med.shimane-u.ac.jp

K. Adachi
Health Center, Shimane Environment and Health Public Corporation, Hamada, Japan

Introduction

Gastroesophageal reflux disease (GERD) is caused by the pathological reflux of gastric contents. Since acidic reflux is the main cause of GERD, inhibition of gastric acid secretion by administration of proton pump inhibitors (PPIs) is widely used as first-line therapy. However, approximately 30 % of treated patients complain about reflux symptoms with PPI use and require additional treatment [1, 2]. As a second-line therapy, mosapride, a prokinetic agent that activates the serotonin 5-HT4 receptor, has been used in clinical practice, though reports concerning its beneficial effects for GERD are conflicting [3–6], as some have shown an augmenting action of mosapride on esophageal peristalsis and lower esophageal sphincter pressure [3–5], while others failed to find those activities [6]. These conflicting results may be derived from the different dosages examined, with higher doses possibly necessary to gain beneficial therapeutic effects.

The esophagogastric junction (EGJ) is an important structure for prevention of gastroesophageal reflux. Patients with GERD show high compliance in this area and their cross-sectional area (CSA) of EGJ during pressure distension is known to be larger than that in normal individuals [7]. Increased EGJ compliance is considered to increase the CSA of the EGJ and diminish air/fluid discrimination during transient lower esophageal sphincter

relaxation-associated reflux with increasing volumes of gastroesophageal fluid reflux, though it does not initiate the reflux events itself [8–12]. In addition, fundoplication surgery has been reported to prevent pathological gastroesophageal reflux by restoring normal EGJ compliance [13].

Drugs that reduce EGJ compliance and decrease the CSA of the EGJ are expected to inhibit pathological gastroesophageal reflux. Recently, an endoluminal functional lumen-imaging probe (FLIP; EndoFLIP®, Crospon Ltd, Galway, Ireland) was shown to be useful for evaluating compliance of the upper and lower esophageal sphincter [7, 14–17]. In the present study, the effects of high-dose mosapride on EGJ compliance and esophageal motor function were investigated using the EndoFLIP system and high-resolution 36-channel manometry in healthy volunteers to test the feasibility of the drug as a possible therapeutic agent for patients with GERD.

Methods

Nine normal healthy male volunteers (age 21–52 years old, mean 35.2 years) without abdominal symptoms were enrolled in this study. After fasting for at least 8 h, a high-resolution 36-channel manometry sensor catheter (ManoScan^{360}; Sierra Scientific Instruments, Los Angeles, CA) was transnasally introduced into the esophagus and esophageal motor activity was measured in a supine position [18]. Next, the manometry catheter was withdrawn and the FLIP device was transnasally inserted in the same manner as the manometry catheter and positioned at the EGJ, then compliance of the EGJ was also measured in a supine position [7, 14–17, 19, 20]. After baseline measurements of esophageal motor activities and EGJ compliance were obtained, mosapride was orally administered. The maximum serum concentration of mosapride is known to be reached at 2.7 h after oral administration and the maximal clinical dose used in Japan is 40 mg in 2 divided doses with a 2-h interval. Therefore, mosapride at 20 mg was orally administered to the volunteers, followed by another 20 mg orally 2 h later. One hour after the second dose, esophageal manometry and EGJ compliance measurements were repeated. Those values obtained before and after mosapride administration were then compared, and analyzed.

The method for dosage of mosapride used in this study is the standard approved method for bowel preparation for colonoscopy in daily clinical practice in Japan. The safety of daily administrations of 120 mg of mosapride has also been reported [21]. The affinity of mosapride for the human ether-a-go-go-related gene (hERG) was reported to be <1000 times that of cisapride, a 5-HT4 receptor agonist that causes electrocardiographic abnormalities [22], and the drug is believed to have a very low risk of causing electrocardiographic abnormalities including QT prolongation [23]. Therefore, we did not perform an electrocardiographic study before or after mosapride administration in our subjects.

Esophageal motor function was evaluated using high-resolution 36-channel manometry according to a previously reported method [6, 24–26]. Based on the manufacturer's instructions, the transducers were calibrated before each measurement. The catheter was inserted transnasally, then the measurements were performed in a supine position starting 5 min after insertion. Resting lower esophageal sphincter (LES) pressure was measured for at least 5 min. Esophageal body peristaltic contractions were measured after drinking 5 ml of water, which was repeated at 2-min intervals until 5 complete contraction records were obtained. According to previous reports, esophageal body peristaltic contractions were separated into 3 segments (oral, middle, lower) [27, 28] (Fig. 1). We determined the maximum peristaltic contraction pressure in each segment and calculated the mean of 5 separate contractions in each subject.

Compliance of the EGJ was determined using an EndoFLIP system [14–17, 19, 20]. The EndoFLIP uses impedance planimetry with 16 electrodes to measure the CSA at 5-mm intervals inside a saline-filled bag (length 80 mm). With this system, the bag is attached to the tip of a catheter probe and can be filled with different volumes of fluid. In addition, the diameter and intra-bag pressure can be simultaneously assessed, and the CSA of the EGJ and intra-bag distensibility pressure are evaluated at the same time. The distension probe and pressure transducers were calibrated based on the manufacturer's instructions. The pressure sensor was set to 0 before insertion of the catheter and then the deflated catheter was transnasally inserted. In our study protocol, the balloon was inflated to volumes of 20, 40, and 50 ml. Peristaltic waves were often visible and ignored, with data obtained as soon as a steady state of a combination of intra-bag pressure, minimum diameter (D_{min}), and CSA was observed with real-time imaging. We recorded diameter (mm), CSA (mm^2), and distensibility indices (DI mm^2/mmHg), as previously reported [14, 19]. The EGJ distensibility index was based on the narrowest CSA in relation to the corresponding intra-bag pressure and calculated with the following equation: [narrowest CSA/(intra-bag pressure + intragastric pressure affects)]. EGJ compliance was successfully measured in all 9 of the volunteers examined in this study.

A Wilcoxon signed rank test was used for statistical comparisons between the mosapride administered and control periods. All calculations were done with Stat View 5.0 software (Abacus Concepts Inc., Berkeley, CA, USA)

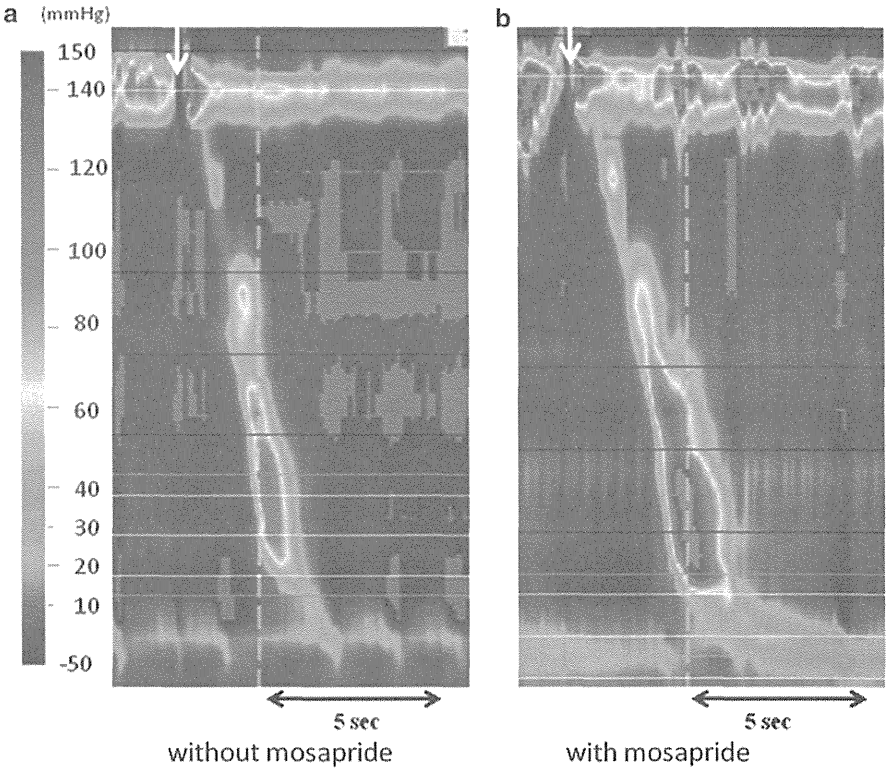

Fig. 1 Pressure tomography observed by high-resolution manometry in a representative subject. Esophageal peristaltic contractions were divided into 3 segments by 2 troughs and the lower segment showed the strongest contractions. Esophageal peristaltic contractions and esophageal resting pressure were higher in the mosapride-treated period (**b**) as compared to the non-treated period (**a**)

for Macintosh. Differences at $P < 0.05$ were considered to be statistically significant.

The study protocol was approved by the ethical committee of Shimane University Faculty of Medicine. Written informed consent was obtained from each of the enrolled volunteers.

Results

Manometry data for 1 volunteer were not obtained because of mechanical trouble, thus the results from 8 were analyzed. The maximal contraction pressure was highest in the lower segment (segment 3) and lowest in the upper segment (segment 1). Mosapride administration tended to increase the peristaltic contraction pressure in segments 1 and 2 (upper and middle segments of esophagus), though the differences did not reach statistical significance. In the lower segment, mosapride given twice (40 mg total dose) resulted in a statistically significant increase in mean maximum contraction pressure (from 130.0 to 147.7 mmHg), as shown in Table 1. In addition, mean LES resting pressure in a supine position increased from 25.0 to 28.9 mmHg following administration of 40 mg of mosapride. Therefore, mosapride at a higher dose was considered to augment esophageal contractions, especially in the distal segments and EGJ areas.

Table 1 Esophageal motor activity ($n = 8$)

	Before administration	After administration
Maximal peristaltic contraction		
Segment 1 (mmHg)	77.2 ± 13.1	83.5 ± 17.2
Segment 2 (mmHg)	112.0 ± 15.2	131.1 ± 22.3
Segment 3 (mmHg)	130.0 ± 18.8	147.7 ± 23.7*
Resting LES pressure (mmHg)	25.0 ± 2.5	28.9 ± 3.7*

Values are expressed as the mean ± SE

* vs. before administration ($P < 0.05$)

The FLIP bag was configured into an hourglass shape when distended to straddle the EGJ, with the central constriction at the diaphragmatic hiatus during both the mosapride treated and non-treated periods. The diaphragmatic hiatus consistently fit to the least distensible locus with a minimal opening diameter (Fig. 2). The hiatal diameter (D_{min}) and CSA progressively increased with distending volume, as did the intra-bag pressure. During the mosapride administration period, intra-bag pressure was higher and the hiatal CSA was lower with the 40- and 50-ml intra-bag volumes ($P < 0.05$), as shown in Table 2. At all distensible pressures, the extent of the EGJ opening during the mosapride treated period was smaller than that during the non-treated period (Fig. 3). Using intra-bag pressure and hiatal CSA, an EGJ distensibility index (DI) was calculated

for each distension volume (Table 2). This index was significantly and consistently lower during administration of mosapride at each distention volume, suggesting a reducing effect of mosapride on EGJ compliance. No statistically significant negative relationship between resting LES pressure and EGJ DI was found.

Discussion

In the present study, high-dose (40 mg) mosapride was found not only to augment peristaltic esophageal body contractions and LES pressure, but also reduce EGJ compliance. The anti-reflux mechanism of the esophagus is composed of 3 different factors. First, the high pressure zone at the LES prevents reflux of gastric contents. Indeed, free and stress-induced gastroesophageal refluxes are known to occur frequently in GERD patients with lowered LES pressure [29, 30]. Next, the limited range of EGJ compliance reduces high volume fluid reflux from the stomach, whereas patients with GERD have been reported to have a higher amount of EGJ compliance in studies using a FLIP device or similar method [7, 12]. Finally, efficient esophageal body peristaltic contractions are important to clear refluxed gastric contents from the esophagus [31–34]. These 3 factors composing the anti-reflux mechanism were investigated in the present study using 2 different techniques; high resolution manometry of the esophagus and the FLIP method.

We enrolled 9 normal volunteers without GERD to assess the feasibility of mosapride as a possible drug to treat PPI-resistant GERD patients. Mosapride stimulates gastrointestinal contractions by activating the serotonin 5-HT4 receptor and releasing acetylcholine from vagal efficient neurons [35]. With its administration, gastric emptying has been reported to be accelerated [36]. Although lower doses of mosapride failed to augment esophageal motor functions [6], higher doses were reported to enhance esophageal contractions [21, 37]. In the present study, a high dose of 40 mg was shown to augment esophageal body peristaltic contractions and suggested to facilitate the esophageal clearance mechanism. In addition, we found that mosapride elevated resting LES pressure with possible efficient protection against stress-induced gastroesophageal reflux. In the present study, esophageal high-resolution manometry revealed the potential anti-GERD action of mosapride in normal individuals.

In addition to augmentation of esophageal contractions, mosapride was found to reduce EGJ compliance. When the FLIP bag was serially inflated at the EGJ, the narrowest

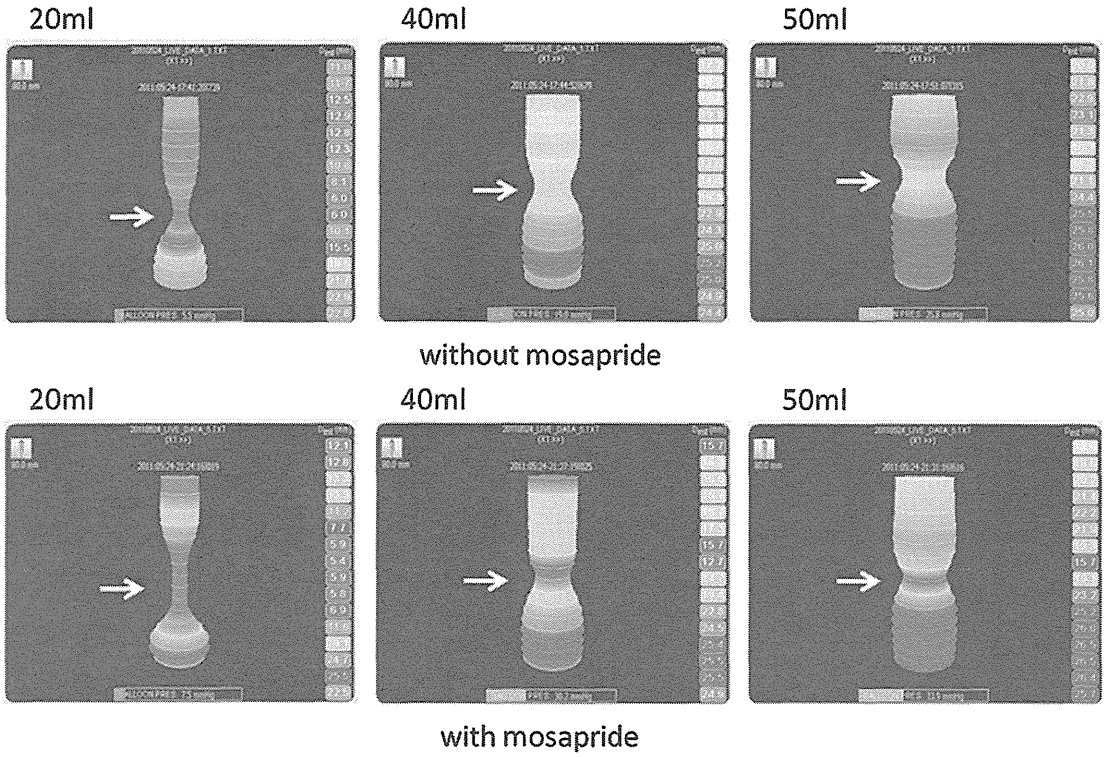

Fig. 2 Shown is a representative set of volumetric FLIP distensions observed during mosapride treated (*lower*) and non-treated (*upper*) periods. The volume number shows the volume of inflated air. EGJ compliance is illustrated as a cylinder of varying diameter with the corresponding intra-bag pressure. The hourglass shape of the EGJ was narrowed at the hiatus (*arrows*). The EGJ became narrower with mosapride treatment

Table 2 Esophagogastric junction compliance ($n = 9$)

	Before administration	After administration
Distention volume, 20 ml		
Minimum diameter (D_{min}) (mm)	5.6 ± 0.3	5.6 ± 0.4
Hiatal CSA (mm^2)	25.2 ± 2.5	25.9 ± 4.8
Intra-bag pressure (mmHg)	10.3 ± 1.4	18.5 ± 3.9**
DI (mm^2/mmHg)	2.9 ± 0.6	2.2 ± 0.7*
Distention volume, 40 ml		
Minimum diameter (D_{min}) (mm)	14.4 ± 0.3	11.4 ± 1.1*
Hiatal CSA (mm^2)	163.0 ± 5.9	110.3 ± 18.5*
Intra-bag pressure (mmHg)	25.9 ± 3.2	31.4 ± 3.2*
DI (mm^2/mmHg)	7.1 ± 0.9	4.1 ± 0.8**
Distention volume, 50 ml		
Minimum diameter (D_{min}) (mm)	18.1 ± 0.4	16.4 ± 0.5**
Hiatal CSA (mm^2)	259.6 ± 12.0	211.9 ± 12.8**
Intra-bag pressure (mmHg)	33.1 ± 2.3	37.1 ± 3.7*
DI (mm^2/mmHg)	8.2 ± 0.8	6.4 ± 0.9**

Values are expressed as the mean ± SE

DI distensibility index

* vs. before administration ($P < 0.05$)

** vs. before administration ($P < 0.01$)

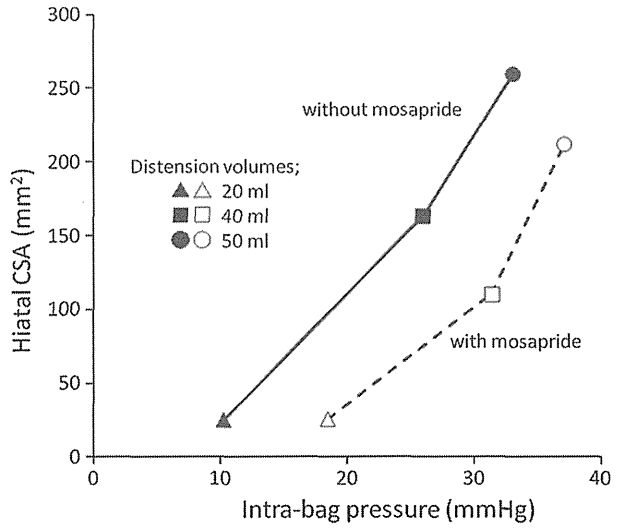

Fig. 3 EGJ compliance with and without 40-mg mosapride administration. FLIP bag pressure (*x*-axis) and hiatal CSA (*y*-axis) were measured with the FLIP bag filled to 20 ml (*triangles*), 40 ml (*squares*), and 50 ml (*circles*) of fluid. Intra-bag pressures were consistently higher at similar hiatal CSA values with administration of mosapride, suggesting reduced EGJ compliance

part of the hiatus gradually widened both before and during mosapride administration. The intra-bag pressure was higher with the same intra-bag volume during mosapride treatment, while the CSA of the narrowest hiatal locus was smaller. These changes in minimal diameter at the hiatal locus also showed a similar trend with those of the hiatal CSA. Together, our results indicated that intraluminal pressure-induced distension of the EGJ was reduced by mosapride administration, suggesting its effect to produce a stronger EGJ barrier against high volume fluid reflux.

The relationship between LES pressure and EGJ compliance is an interesting point to be investigated. Although we did not find a statistically significant relationship between these two parameters, probably because of the small size of the study population, Pandolfino et al. [12] reported a weak negative relationship between them. Based on their results, they concluded that basal LES pressure likely plays only a small role in determining compliance of the EGJ. Further study is required to clarify the relationship between resting LES pressure and EGJ compliance.

In our study, we found beneficial effects of mosapride on esophageal motor activities and EGJ compliance. In addition to the esophagus, this drug has been reported to stimulate gastric motor activity and gastric emptying [38, 39]. Accelerated gastric emptying is believed to decrease postprandial gastroesophageal reflux through several mechanisms and may have beneficial effect on patients with GERD. In addition, recent findings indicate that mosapride facilitates early absorption of PPIs by accelerating drug emptying to the small intestine and elevating intragastric pH more quickly after PPI administration [40]. Therefore, the combined effects of mosapride on the esophagus and stomach should be considered when evaluating the drug in patients with GERD.

This is the first study to show a diminishing effect of mosapride on EGJ compliance. During mosapride administration, EGJ opening during pressure distension is limited, which is thought to decrease the volume of refluxate and limit upper esophageal reflux. We previously reported that mosapride administration in patients treated by percutaneous gastrostomy liquid nutrient feeding remarkably decreased the occurrence of aspiration pneumonia caused by gastroesophageal reflux [41]. We consider that the effects of mosapride on EGJ compliance found in the present study provide important information for understanding the mechanism of these gastroesophageal reflux-related diseases.

There are some limitations to our study. First, the subjects were 9 normal individuals without GERD. In addition, we did not investigate the direct effects of mosapride on gastroesophageal reflux, because of the limited reflux present in our normal volunteers. The effects of a 40-mg dose of mosapride on gastroesophageal reflux were previously reported in cases with GERD [37], and those findings clearly indicated that mosapride decreased the number of esophageal acid reflux events as well as their extent. Therefore, we believe that similar effects of mosapride on esophageal motor activity and EGJ compliance occur in patients with GERD as in normal individuals. Indeed, an

augmenting effect of mosapride on esophageal peristaltic contractions in GERD patients has been reported [21, 42]. Another limitation is that the method for dosage of mosapride in our study might be impossible for GERD patients in routine clinical practice. Nevertheless, our findings suggest the possible value of mosapride as a research target for potential use in PPI-resistant GERD patients and further studies are recommended to demonstrate the efficacy of high-dose mosapride on GERD-related gastroesophageal reflux.

In summary, mosapride, a prokinetic drug featuring 5-HT4 stimulation, at a dose of 40 mg reduced EGJ compliance, and also augmented esophageal body peristalsis and LES pressure.

Acknowledgments Kousuke Fukazawa, Kenji Furuta, Kyoichi Adachi, Yoshiya Moritou, Tsukasa Saito, Ryusaku Kusunoki, Goichi Uno, Shino Shimura, Masahito Aimi, Shunji Ohara, and Shunji Ishihara performed the research; Kousuke Fukazawa, Kenji Furuta, Kyoichi Adachi, Shunji Ishihara, and Yoshikazu Kinoshita designed the research study; Kousuke Fukazawa, Masahito Aimi, and Yoshikazu Kinoshita contributed essential tools; Kousuke Fukazawa, Kenji Furuta, Shino Shimura, Masahito Aimi, Shunji Ohara, and Kyoichi Adachi analyzed the data; and Kousuke Fukazawa, Kenji Furuta, Kyoichi Adachi, and Yoshikazu Kinoshita wrote the paper. This work was supported by a research fund of Shimane University Faculty of Medicine.

Conflict of interest The authors declare that they have no conflict of interest.

References

1. Adachi K, Furuta K, Miwa H, Oshima T, Miki M, Komazawa Y, et al. A study on the efficacy of rebamipide for patients with proton pump inhibitor-refractory non-erosive reflux disease. Dig Dis Sci. 2012;57:1609–17.
2. Fass R. Therapeutic options for refractory gastroesophageal reflux disease. J Gastroenterol Hepatol. 2012;27(Suppl 3):3–7.
3. Hsu YC, Lin HJ. Addition of prokinetic therapy to a PPI in reflux diseases. Aliment Pharmacol Ther. 2011;33:983–4.
4. Miwa H, Inoue K, Ashida K, Kogawa T, Nagahara A, Yoshida S, et al. Randomised clinical trial: efficacy of the addition of a prokinetic, mosapride citrate, to omeprazole in the treatment of patients with non-erosive reflux disease—a double-blind, placebo-controlled study. Aliment Pharmacol Ther. 2011;33:323–32.
5. Madan K, Ahuja V, Kashyap PC, Sharma MP. Comparison of efficacy of pantoprazole alone versus pantoprazole plus mosapride in therapy of gastroesophageal reflux disease: a randomized trial. Dis Esophagus. 2004;17:274–8.
6. Koshino K, Adachi K, Furuta K, Ohara S, Morita T, Nakata S, et al. Effects of mosapride on esophageal functions and gastroesophageal reflux. J Gastroenterol Hepatol. 2010;25:1066–71.
7. Kwiatek MA, Pandolfino JE, Hirano I, Kahrilas PJ. Esophagogastric junction distensibility assessed with an endoscopic functional luminal imaging probe (EndoFLIP). Gastrointest Endosc. 2010;72:272–8.
8. Ghosh SK, Kahrilas PJ, Brasseur JG. Liquid in the gastroesophageal segment promotes reflux, but compliance does not: a mathematical modeling study. Am J Physiol Gastrointest Liver Physiol. 2008;295:G920–33.
9. Jenkinson AD, Scott SM, Yazaki E, Fusai G, Walker SM, Kadirkamanathan SS, et al. Compliance measurement of lower esophageal sphincter and esophageal body in achalasia and gastroesophageal reflux disease. Dig Dis Sci. 2001;46:1937–42.
10. Pandolfino JE, Shi G, Curry J, Joehl RJ, Brasseur JG, Kahrilas PJ. Esophagogastric junction distensibility: a factor contributing to sphincter incompetence. Am J Physiol Gastrointest Liver Physiol. 2002;282:G1052–8.
11. Kahrilas PJ, Shi G, Manka M, Joehl RJ. Increased frequency of transient lower esophageal sphincter relaxation induced by gastric distention in reflux patients with hiatal hernia. Gastroenterology. 2000;118:688–95.
12. Pandolfino JE, Shi G, Trueworthy B, Kahrilas PJ. Esophagogastric junction opening during relaxation distinguishes nonhernia reflux patients, hernia patients, and normal subjects. Gastroenterology. 2003;125:1018–24.
13. Pandolfino JE, Curry J, Shi G, Joehl RJ, Brasseur JG, Kahrilas PJ. Restoration of normal distensive characteristics of the esophagogastric junction after fundoplication. Ann Surg. 2005;242:43–8.
14. Nathanson LK, Brunott N, Cavallucci D. Adult esophagogastric junction distensibility during general anesthesia assessed with an endoscopic functional luminal imaging probe (EndoFLIP®). Surg Endosc. 2012;26:1051–5.
15. Rohof WO, Hirsch DP, Kessing BF, Boeckxstaens GE. Efficacy of treatment for patients with achalasia depends on the distensibility of the esophagogastric junction. Gastroenterology. 2012;143:328–35.
16. Rieder E, Swanström LL, Perretta S, Lenglinger J, Riegler M, Dunst CM. Intraoperative assessment of esophagogastric junction distensibility during per oral endoscopic myotomy (POEM) for esophageal motility disorders. Surg Endosc. 2013;27:400–5.
17. Perretta S, Dallemagne B, McMahon B, D'Agostino J, Marescaux J. Improving functional esophageal surgery with a "smart" bougie: Endoflip. Surg Endosc. 2011;25:3109.
18. Bhatia SJ, Shah C. How to perform and interpret upper esophageal sphincter manometry. J Neurogastroenterol Motil. 2013;19:99–103.
19. Regan J, Walshe M, Rommel N, Tack J, McMahon BP. New measures of upper esophageal sphincter distensibility and opening patterns during swallowing in healthy subjects using EndoFLIP®. Neurogastroenterol Motil. 2013;25:e25–34.
20. Alqudah MM, Gregersen H, Drewes AM, McMahon BP. Evaluation of anal sphincter resistance and distensibility in healthy controls using EndoFLIP©. Neurogastroenterol Motil. 2012;24:e591–9.
21. Ruth M, Finizia C, Cange L, Lundell L. The effect of mosapride on oesophageal motor function and acid reflux in patients with gastro-oesophageal reflux disease. Eur J Gastroenterol Hepatol. 2003;15:1115–21.
22. Toga T, Kohmura Y, Kawatsu R. The 5-HT(4) agonists cisapride, mosapride, and CJ-033466, a Novel potent compound, exhibit different human ether-a-go-go-related gene (hERG)-blocking activities. J Pharmacol Sci. 2007;105:207–10.
23. Endo J, Nomura M, Morishita S, Uemura N, Inoue S, Kishi S, et al. Influence of mosapride citrate on gastric motility and autonomic nervous function: evaluation by spectral analyses of heart rate and blood pressure variabilities, and by electrogastrography. J Gastroenterol. 2002;37:888–95.
24. Yoshida K, Furuta K, Adachi K, Ohara S, Morita T, Tanimura T, et al. Effects of anti-hypertensive drugs on esophageal body contraction. World J Gastroenterol. 2010;16:987–91.
25. Fox MR, Bredenoord AJ. Oesophageal high-resolution manometry: moving from research into clinical practice. Gut. 2008;57:405–23.

26. Salvador R, Dubecz A, Polomsky M, Gellerson O, Jones CE, Raymond DP, et al. A new era in esophageal diagnostics: the image-based paradigm of high-resolution manometry. J Am Coll Surg. 2009;208:1035–44.
27. Clouse RE, Staiano A. Topography of the esophageal peristaltic pressure wave. Am J Physiol. 1991;261:G677–84.
28. Clouse RE, Staiano A. Topography of normal and high-amplitude esophageal peristalsis. Am J Physiol. 1993;265:G1098–107.
29. Dodds WJ, Dent J, Hogan WJ, Helm JF, Hauser R, Patel GK, et al. Mechanisms of gastroesophageal reflux in patients with reflux esophagitis. N Engl J Med. 1982;307:1547–52.
30. Dodds WJ. The pathogenesis of gastroesophageal reflux disease. AJR Am J Roentgenol. 1988;151:49–56.
31. Ho SC, Chang CS, Wu CY, Chen GH. Ineffective esophageal motility is a primary motility disorder in gastroesophageal reflux disease. Dig Dis Sci. 2002;47:652–6.
32. Wong WM, Lai KC, Hui WM, Hu WH, Huang JQ, Wong NY, et al. Pathophysiology of gastroesophageal reflux diseases in Chinese—role of transient lower esophageal sphincter relaxation and esophageal motor dysfunction. Am J Gastroenterol. 2004;99:2088–93.
33. Chitkara DK, Fortunato C, Nurko S. Esophageal motor activity in children with gastro-esophageal reflux disease and esophagitis. J Pediatr Gastroenterol Nutr. 2005;40:70–5.
34. Iwakiri K, Kawami N, Sano H, Tanaka Y, Umezawa M, Kotoyori M, et al. Mechanisms of excessive esophageal acid exposure in patients with reflux esophagitis. Dig Dis Sci. 2009;54:1686–92.
35. Makimoto N, Sakurai-Yamashita Y, Furuichi A, Kawakami S, Enjoji A, Kanematsu T, et al. In vivo assessment of acceleration of motor activity associated with acetylcholine release via 5-hydroxytryptamine. Jpn J Pharmacol. 2002;90:28–35.
36. Kawamura E, Enomoto M, Kotani K, Hagihara A, Fujii H, Kobayashi S, et al. Effect of mosapride citrate on gastric emptying in interferon-induced gastroparesis. Dig Dis Sci. 2012;57:1510–6.
37. Ruth M, Hamelin B, Röhss K, Lundell L. The effect of mosapride, a novel prokinetic, on acid reflux variables in patients with gastro-oesophageal reflux disease. Aliment Pharmacol Ther. 1998;12:35–40.
38. Kusunoki H, Haruma K, Hata J, Kamada T, Ishii M, Yamashita N, et al. Efficacy of mosapride citrate in proximal gastric accommodation and gastrointestinal motility in healthy volunteers: a double-blind placebo-controlled ultrasonographic study. J Gastroenterol. 2010;45:1228–34.
39. Sakamoto Y, Sekino Y, Yamada E, Ohkubo H, Higurashi T, Sakai E, et al. Mosapride accelerates the delayed gastric emptying of high-viscosity liquids: a crossover study using continuous real-time C breath test (BreathID System). J Neurogastroenterol Motil. 2011;17:395–401.
40. Iida H, Inamori M, Fujii T, Sekino Y, Endo H, Hosono K, et al. Early effect of oral administration of omeprazole with mosapride as compared with those of omeprazole alone on the intragastric pH. BMC Gastroenterol. 2012;12:25.
41. Takatori K, Yoshida R, Horai A, Satake S, Ose T, Kitajima N, et al. Therapeutic effects of mosapride citrate and lansoprazole for prevention of aspiration pneumonia in patients receiving gastrostomy feeding. J Gastroenterol 2012. [Epub ahead of print].
42. Cho YK, Choi MG, Park EY, Lim CH, Kim JS, Park JM, et al. Effect of mosapride combined with esomeprazole improves esophageal peristaltic function in patients with gastroesophageal reflux disease: a study using high resolution manometry. Dig Dis Sci. 2013;58:1035–41.

Role of Regulatory B Cells in Chronic Intestinal Inflammation: Association with Pathogenesis of Crohn's Disease

Akihiko Oka, MD, Shunji Ishihara, MD, PhD,* Yoshiyuki Mishima, MD, PhD,* Yasumasa Tada, MD,* Ryusaku Kusunoki, MD,* Nobuhiko Fukuba, MD,* Takafumi Yuki, MD, PhD,† Kousaku Kawashima, MD, PhD,* Satoshi Matsumoto, PhD,‡ and Yoshikazu Kinoshita, MD, PhD**

Abstract: The role of regulatory B cells (Bregs) producing interleukin (IL)-10 in the pathogenesis of inflammatory bowel diseases remains unknown. We investigated IL-10 production in B cells from patients with inflammatory bowel diseases and immunoregulatory functions of Bregs in experimental colitis mouse models. CpG DNA-induced IL-10 production in peripheral blood B cells isolated from patients with inflammatory bowel diseases and control subjects was examined. CD19 and CD1d were used for evaluating possible cell surface markers of Bregs. Colitis models of severe combined immunodeficiency mice were established by adoptive transfer of whole $CD4^+$ T cells or regulatory T cell (Treg)-depleted T cells ($CD4^+CD25^-$) isolated from SAMP1/Yit mice and the function of Bregs in intestinal inflammation was elucidated by evaluating the effects of cotransfer of whole or Breg-depleted B cells. CpG DNA-induced IL-10 production was significantly decreased in B cells from patients with Crohn's disease (CD), as compared with those from healthy controls, whereas Bregs were found to be enriched in a population of $CD19^{hi}$ and $CD1d^{hi}$ B cells isolated from both human and mouse samples. The severity of intestinal inflammation was significantly increased in the Breg-depleted mice, with similar results also found in adoptive transfer colitis model mice even after Treg depletion. Our findings show that Bregs, characterized by the cell surface markers $CD19^{hi}$ and $CD1d^{hi}$, significantly reduced experimental colitis regardless of the presence or absence of Tregs. These results suggest that a deficiency or decrease of Bregs function exacerbates intestinal inflammation, which may be associated with the pathogenesis of CD.

(Inflamm Bowel Dis 2014;20:315–328)

Key Words: regulatory B cells, inflammatory bowel disease, intestinal inflammation, innate immunity

Crohn's disease (CD) is a chronic intestinal immune-mediated disorder characterized by a relapsing–remitting course. Although its etiology is not fully understood, various genes indicating susceptibility for CD have been recently identified in familial and candidate gene assays and several genome-wide association studies.[1] Findings of expression of those genes and analysis of their functions, as well as experiments using gene targeting in animals suggest that the involvement of these genes in the pathogenesis of CD is closely associated with the dysfunctions of host innate and adaptive immune systems.[2,3] In this regard, studies focused on the functions of gut immune cells are crucial for understanding the pathogenesis of the disease.

B cells typically play important immune roles, including antibody production, antigen presentation, costimulation with T cells, and cytokine production. Disorders of B cells in relation to excess host immune responses have been widely investigated in numerous studies to elucidate the pathogenesis of various inflammatory and autoimmune diseases.[4–8] In addition to those roles of conventional B cells, recent studies have shown that a novel subset of B cells has unique immune regulatory functions to modulate inflammation and autoimmunity.[9–13] This subset is currently considered to consist of regulatory B cells (Bregs), which is characterized by the production of the regulatory cytokine interleukin (IL)-10 and transforming growth factor (TGF)-β.[14] Bregs have been reported to contribute to host immune regulation by activating regulatory T cells (Tregs), regulating Th1/Th2 cytokine balance and dendritic cell functions, downregulating the proinflammatory network, and suppressing T cell-mediated autoimmunity.[8–19] Furthermore, lack or dysfunction of this regulatory subset of B cells has been demonstrated to develop or exacerbate various autoimmune diseases.[6,8,10,20,21]

SAMP1/Yit (SAMP1) mice spontaneously develop intestinal inflammation in the ileum and cecum and are widely recognized as a murine model of CD.[22] We recently investigated the role of B cells in the pathogenesis of ileitis using SAMP1 mice and found that CpG DNA-stimulated IL-10 production in the

Supplemental digital content is available for this article. Direct URL citations appear in the printed text and are provided in the HTML and PDF versions of this article on the journal's Web site (www.ibdjournal.org).

Received for publication October 7, 2013; Accepted October 29, 2013.

From the *Department of Internal Medicine II, Shimane University School of Medicine, Shimane, Japan; †Division of Gastrointestinal Endoscopy, Shimane University Hospital, Shimane, Japan; and ‡Yakult Central Institute for Microbiological Research, Tokyo, Japan.

Supported in part by Health and Labour Sciences Research Grants for research of intractable diseases from the Ministry of Health, Labour, and Welfare of Japan.

The authors have no conflicts of interest to disclose.

Reprints: Shunji Ishihara, MD, PhD, Department of Internal Medicine II, Shimane Medical University, 89-1, Enya-cho, Izumo, 693-8501, Shimane, Japan (e-mail: si360405@med.shimane-u.ac.jp).

DOI 10.1097/01.MIB.0000437983.14544.d5

Published online 2 January 2014.

cultured B cells isolated from mesenteric lymph nodes (MLNs) of those mice was significantly decreased as compared with control mice.[23] In addition, increased production of IL-1β and interferon-γ by activated macrophages and T cells was noted only when they were cocultured with MLN B cells of SAMP1 mice. These findings suggested that the dysfunction of this regulatory subset of B cells may induce intestinal inflammation, which might be associated with the pathogenesis of CD.

In this study, 2 experimental protocols were designed to further clarify the role of Bregs in the pathogenesis of CD. First, we isolated peripheral blood B cells from patients with CD and examined CpG DNA-induced IL-10 production in those cultured cells and then compared the results with B cells from patients with ulcerative colitis (UC) and healthy control subjects. Next, we established a CD model of severe combined immunodeficiency (SCID) mice by adoptive transfer of $CD4^+$ T cells isolated from the SAMP1 strain and investigated the regulatory role of B cells in intestinal inflammation by evaluating the effects of cotransfer of total or Breg-depleted B cells. Our results showed that CpG DNA-stimulated IL-10 production in B cells was decreased in patients with CD, whereas the lack of Bregs exacerbated intestinal inflammation in the SCID adoptive transfer colitis model, suggesting that dysregulation of Bregs may be associated with the pathogenesis of CD.

MATERIALS AND METHODS

Reagents

We used the following antibodies (Abs) for flow cytometry: APC-, FITC-, PE-, and PE-Cy5–conjugated or purified anti–human CD1d (eBioscience, San Diego, CA), CD4 (Miltenyi Biotec, Auburn, CA), CD19 (Beckman Coulter, Brea, CA), CD19, CD24, CD38 (BD Biosciences-Pharmingen, San Jose, CA), IL-10 (R&D Systems, Minneapolis, AL), anti–mouse CD4, CD11c (Miltenyi Biotec), CD19, CD1d, IL-10 (BD Biosciences-Pharmingen), and IgG isotypes (R&D Systems). Fc receptors were blocked with anti-CD32 (Miltenyi Biotec). We also used anti–mouse CD4, CD19, CD25, and anti–human CD19 microbeads (Miltenyi Biotec). For intracellular cytokine staining, brefeldin A (Sigma–Aldrich, Saint Louis, MO) or GolgiStop (BD Biosciences-Pharmingen) was used. Phorbol 12-myristate 13-acetate and ionomycin were obtained from Sigma–Aldrich. Ultra pure *Escherichia coli* lipopolysaccharide (LPS) (0111:B4 strain) was obtained from GIBCO-Invitrogen (San Diego, CA). Unmethylated CpG DNA (5'-TGACTGTGAACGTTCGAGATGA-3') was synthesized by Hokkaido System Science Co., Ltd. Enzyme immunoassays (EIA) kits for Quantikine mouse IL-6, IL-10, and tumor necrosis factor (TNF)-α, and human IL-10 immunoassays were obtained from R&D Systems. The anti–mouse IL-10 antibody (BD Biosciences-Pharmingen) was used after depleting azide. For immunohistochemistry, anti–mouse CD3, CD19 (Cell Signaling Technology, Tokyo, Japan), and Foxp3 (Life Span Biosciences, Seattle, WA) were used.

Flow Cytometry

The above human and mouse Abs were used for flow cytometry analyses as necessary. Fc receptors were blocked with anti–CD32 (2.4G2) Abs, and brefeldin A or GolgiStop was added to the medium during the last 5 hours of the culture period for intracellular cytokine staining. Flow cytometry analysis was performed using an FACS Aria II (BD Biosciences-Pharmingen) or EPICS XL (Beckman Coulter, Tokyo, Japan).

Human Samples

Peripheral whole blood samples were obtained from patients with inflammatory bowel disease (IBD), 18 with CD and 23 with UC, and 26 healthy control subjects. The diagnosis of IBD was based on clinical, endoscopic, histological, and radiological features. The activities of CD and UC were determined using the Crohn's disease activity index and the Rachmilewitz clinical activity index, respectively. Peripheral blood leukocyte subsets and serum C-reactive protein levels were examined using routine laboratory techniques at Shimane University Hospital. The study protocol was approved by the Ethics Committee of Shimane University, and written informed consent was obtained from all subjects.

Purification of Human B Cells and Study Design

Peripheral blood mononuclear cells (PBMCs) were isolated using a Ficoll–Hypaque density gradient (Lymphoprep; AXIS-SHIELD, Oslo, Norway). B cells were magnetically separated from PBMCs by positive selection with CD19 microbeads. Using flow cytometry, the final $CD19^+$ cell fraction was confirmed to be >97% pure and contained <1% $CD4^+$ and <1% $CD11c^+$ cells. Cell viability was shown to be >95% before culturing using a Trypan blue exclusion test. Purified B cells (2×10^6 cells per milliliter) were grown in RPMI 1640 medium (GIBCO-Invitrogen), supplemented with 10% fetal bovine serum (ICN Biomedicals, Aurora, OH) and penicillin–streptomycin–amphotericin B (GIBCO-Invitrogen) and then maintained at 37°C in 5% CO_2 in a humidified incubator. Cultured B cells (4×10^5 cells per well in 96-well plates) were stimulated with CpG DNA (10 nM) for 72 hours. After the cell cultures, supernatants were collected for the measurements of IL-10 contents by EIA, and cells were collected for flow cytometry analysis. Multiple regression analysis was used to determine significant factors affecting the production of IL-10 in CpG DNA-stimulated B cells from patients with IBD in association with clinical parameters. For intracellular staining of IL-10, PBMCs from patients with IBD and healthy subjects were cultured for 24 hours with CpG DNA (10 nM) and then restimulated with phorbol 12-myristate 13-acetate (50 ng/mL) and ionomycin (500 ng/mL), as well as GolgiStop (2 μM) for the final 5 hours.

Mice

SAMP1 mice were kindly provided by S. Matsumoto (Yakult Central Institute for Microbiological Research, Tokyo, Japan). AKR/N (AKR) mice were purchased from Japan SLC, Inc. (Hamamatsu, Japan). AKR mice share a genetic background

with SAMP1 mice and their entire MHC region is identical. SCID mice (CB17/Icr-Prkdc^{scid}/CrlCrlj) were purchased from Charles River Japan, Inc. (Kanagawa, Japan). All experiments with animals in this study were approved by the Ethics Committee for Animal Experimentation of Shimane University and they were handled according to our institutional guidelines.

Establishment of Adoptive Transfer Colitis Models in the Presence or Absence of Tregs

Kosiewicz et al[24] established an SAMP1 adoptive transfer model of CD using C3HSmn and C-Prkdc^{scid}/J SCID mice. In this study, according to their method, we established an adoptive transfer model using SCID mice, in which whole CD4$^+$ T cells were isolated magnetically from MLNs of SAMP1 mice (30–50 weeks old) by positive selection with CD4 microbeads. Isolated whole CD4$^+$ T cells (5×10^5 per mouse) were injected intraperitoneally into SCID mice (8–10 weeks old) to induce intestinal inflammation. Furthermore, we established an additional adoptive transfer colitis model to evaluate whether the function of Bregs is dependent on the presence of Tregs. For creating this model, Treg-depleted T cells (CD4$^+$CD25$^-$) were magnetically isolated by negative selection with CD25 and positive selection with CD4 microbeads. The colitis model in the absence of Tregs was created by injecting isolated CD4$^+$CD25$^-$ T cells (5×10^5 per mouse). Using flow cytometry, each fraction of isolated CD4$^+$ or CD4$^+$CD25$^-$ T cells was confirmed to be >97% pure with <1% CD11c$^+$ cells. Appropriate development of intestinal inflammation in each model was assessed by macroscopic and histological findings. To ensure reconstitution of the transferred lymphocytes, flow cytometry analysis was performed on 28 days after transfer of CD4$^+$ T and CD19$^+$ B cells. The spleen, MLNs, stomach, and small (upper and lower half) and large intestines were harvested, and the single-cell suspensions stained with appropriate Abs were analyzed using flow cytometry. Lamina propria lymphocytes were isolated using a 44% to 70% discontinuous Percoll gradient (GE Healthcare, Buckinghamshire, United Kingdom) described previously.[23]

Sorting of B Cells and Cotransfer Studies

Total MLN B cells were isolated by positive selection with CD19 microbeads from AKR mice (15–25 weeks old). The Breg-rich population was detected based on the presence of the cell surface markers CD19^{hi} and CD1d^{hi}, and depletion from the total population of MLN-derived CD19$^+$ B cells was determined using an FACS sorting system. For investigating the role of Bregs in intestinal inflammation, whole or CD19^{hi} and CD1d^{hi}-depleted B cells (2×10^6 per mouse) were intravenously (tail vein) cotransferred into the above T cell-mediated colitis models. Body weight (BW) changes were monitored weekly using a top-loading balance. All mice were killed at 6 or 7 weeks after cell transfer, and the severity of colitis was examined using the disease activity parameters, BW and histological score. The expression levels of macrophage inflammatory protein-2, interferon-γ, tumor necrosis factor (TNF)-α and IL-1β in intestinal tissues and MLNs were determined using real-time PCR.

Anti-inflammatory Effects of Bregs Associated with IL-10 In Vitro

CD4$^+$CD25$^-$ T cells were magnetically isolated from MLNs of SCID mice transferred with SAMP1 CD4$^+$ T cells (21 days after transfer). T cells (2×10^5 cells per well) were cocultured with whole CD19$^+$ B cells or Breg-depleted CD19$^+$ B cells (2×10^5 cells per well) isolated from MLNs of AKR mice in anti–CD3 antibody-coated 96-well plates (BD Biosciences-Pharmingen) with CpG DNA (10 nM). The effect of the anti–IL-10 antibody (10 μg/mL) was also examined. The supernatants were analyzed by EIA for the detection of TNF-α.

EIA

The concentrations of human IL-10 and murine IL-6, IL-10 and TNF-α were measured in cell culture supernatants using each specific EIA kit, according to the manufacturer's instructions.

Histological Examination

Tissues were formalin-fixed and embedded in paraffin blocks. For histological examinations, 3-μm paraffin sections were stained with hematoxylin and eosin to visualize their general morphology under a light microscope. Histological grading was evaluated as described previously.[25] Three different parameters were examined: active inflammation (neutrophil infiltration of tissue), chronic inflammation (lymphocytes, plasma cells, and macrophages in mucosa and submucosa), and villus distortion (flattening and/or widening of normal mucosal villous architecture). The final score for these 3 parameters was determined by multiplying the histological grade by the numerical assessment of the involved area.

Immunohistochemistry

Frozen tissue samples were sliced into 6-μm thick sections and fixed in cold acetone for 10 minutes. After blocking endogenous peroxidase activity with 0.3% hydrogen peroxide in methanol, the sections were incubated for 2 hours at room temperature with a primary Ab (anti–mouse CD19) at a dilution of 1/100 and processed using the corresponding protocol with an immunoperoxidase staining kit (Vectastain Elite ABC Kit; Vector Laboratories, Burlingame, CA). The secondary Ab was goat anti–rabbit IgG (Imgenex Biotech, Orissa, India). Sections were counterstained with hematoxylin and viewed under a light microscope. Formalin-fixed paraffin-embedded tissue samples (3-μm thick) were deparaffinized using xylene. After antigen retrieval, the sections were incubated for 30 minutes at room temperature with the primary antibody (anti–mouse Foxp3) at a dilution of 1/1000 and then processed using the appropriate corresponding protocol with an immunoperoxidase staining kit (Dako).

RNA Extraction and Real-Time PCR

Total RNA was extracted from each sample using an RNeasy Protect Mini Kit (Qiagen Inc., Tokyo, Japan), and then

equal amounts of RNA were reverse transcribed into cDNA using a QPCR cDNA Kit (Stratagene, La Jolla, CA). All primers (see Table, Supplemental Digital Content 1, http://links.lww.com/IBD/A357, which shows the primer sequences) used were flanked by intron–exon junctions using the NCBI blast tool and the Primer3 software. Quantitative real-time PCR was performed using an ABI PRISM 7700 sequence detection system with SYBR Green PCR master mix (Applied Biosystems, Foster City, CA), according to the manufacturer's instructions. The levels of mRNA were normalized to that of GAPDH using sequence detector software (Applied Biosystems).

Statistical Analysis

All results are expressed as the mean with the standard error of the mean or as a range when appropriate. Student's *t* test and Spearman's rank correlation coincidence were used as appropriate to examine significant differences. *P* values <0.05 were considered as statistically significant. All statistical analyses were performed using Statistical Analysis Software (SPSS, version 12.0 for the PC; SPSS Japan Inc., Tokyo, Japan).

RESULTS

Human Studies

Decreased IL-10 Production in CpG DNA-stimulated Peripheral Blood B Cells from Patients with CD

We designed experiments using human peripheral blood B cells isolated from healthy individuals and patients with IBD. Isolated B cells were stimulated with various concentrations of LPS or CpG DNA at different time points. CpG DNA significantly induced IL-10 production in human peripheral blood B cells in dose- and time-dependent manners, whereas those effects were weak in LPS-stimulated B cells (data not shown). To further clarify the difference of CpG DNA-induced IL-10 production in B cells between healthy and patients with IBD, peripheral blood B cells were isolated from 26 healthy controls and patients with IBD (CD and UC) (Table 1). The mean levels of IL-10 contents in culture supernatants were significantly lower in those from the patients with CD and UC as compared with the controls (Fig. 1A). In addition, a decreased frequency of IL-10–producing peripheral blood B cells was also observed among cells obtained from the patients with IBD (Fig. 1B). Because the patients with IBD enrolled in this study had various clinical backgrounds including therapeutic regimens, we used multiple regression analysis to determine significant factors affecting CpG DNA-induced IL-10 production in B cells from those patients. Among several clinical parameters examined, the presence of CD was significantly related to decreased production of IL-10 by peripheral blood B cells (Table 2).

Decreased Frequency of $CD19^{hi}CD1d^{hi}$ IL-10–producing B Cells in Patients with CD

To determine possible cell surface markers characterizing the production of IL-10 by B cells, we focused on CD19 and CD1d and evaluated their expressions using flow cytometry. Among the human peripheral blood B cells, IL-10–producing cells were mainly detected by the presence of the cell surface markers $CD19^{hi}CD1d^{hi}$ (Fig. 1B), whereas IL-10 was also found to be expressed in a small number of $CD19^{low\text{-}mid}CD1d^{hi}$ B cells. Furthermore, a decreased frequency of IL-10–producing $CD19^{hi}CD1d^{hi}$ B cells was found in patients with CD (Fig. 1B). Using a method recently reported by Blair et al, we also analyzed

TABLE 1. Characteristics of the Subjects

	CD (n = 18)	UC (n = 23)	Healthy (n = 26)	*P*
Age (range)	36.7 (23–63)	42.9 (17–71)	38.9 (25–72)	n.s.
Male:Female	12:6	15:8	18:8	n.s.
Disease activity (range)	CDAI: 50.8, (13–146)	CAI: 2.28, (0–4)	—	—
5-aminosalycylic acid	17	23	—	—
Corticosteroid	0	7	—	—
Azathioprine	2	4	—	—
Infliximab	6	0	—	—
Apheresis	0	3	—	—
Elemental diet	10	0	—	—
WBC per μL of blood	6494	6378	6168	n.s.
B cell per μL of blood	110	85.7*	167	<0.01
CRP (mg/dL)	0.33†	0.09	0.09	<0.01

CDAI, Crohn's disease activity index; CAI, clinical activity index; WBC, white blood cell; CRP, C-reactive protein (normal range: <0.2 mg/dL); n.s., not significant.
*Versus healthy.
†Versus UC or healthy.

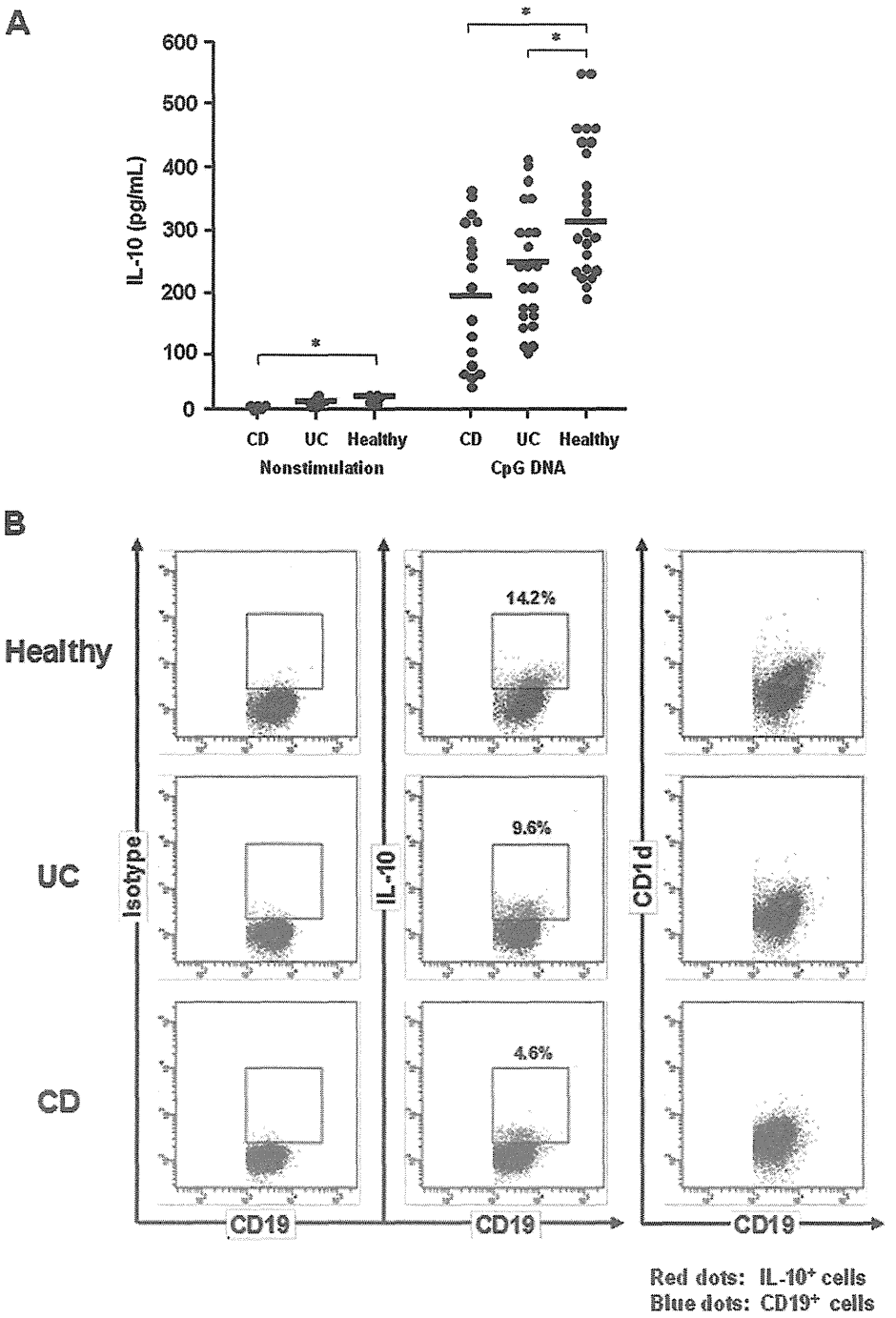

FIGURE 1. Decreased production of IL-10 in peripheral blood B cells from patients with IBD. Peripheral blood B cells were magnetically isolated from 26 healthy controls and patients with IBD (18 with CD and 23 with UC) and incubated at 2×10^6 cells per milliliter (4×10^5 cells per well in 96-well plates) for 72 hours in medium alone or with CpG DNA (10 nM). IL-10 contents in culture supernatants were examined by EIA. The expressions of CD19, CD1d, and IL-10 in B cells were assessed by flow cytometry. The characteristics of the subjects are summarized in Table 1. A, Decreased production levels of IL-10 in peripheral blood B cells from patients with IBD cultured with CpG DNA (10 nM), phorbol 12-myristate 13-acetate (50 ng/mL), and ionomycin (500 ng/mL) (*$P < 0.01$). B, The number of B cells expressing IL-10 was decreased in the patients with IBD. Representative flow cytometry findings showing the expressions of CD19 (blue dots) and IL-10 (red dots) in B cells are presented. IL-10–producing B cells highly expressed CD19 and CD1d. Representative dot plots showing the expression of IL-10$^+$ B cells (red dots) overlaid onto CD19 and CD1d expressions in B cells are presented.

TABLE 2. Factors Correlated with the Production of IL-10 in Peripheral Blood B Cells

Factor	β-coefficient	t-value	P
Age	−0.047	−0.368	0.713
Gender (male)	0.083	0.685	0.496
CD (yes)	−0.693	−2.863	0.005
UC (yes)	−0.264	−1.267	0.210
5-aminosalycylic acid	−0.155	−0.713	0.478
Corticosteroid	0.209	0.790	0.432
Azathioprine	0.008	0.063	0.949
Infliximab	0.059	0.409	0.683
Apheresis	0.045	0.184	0.854
Elemental diet	0.279	1.919	0.060
Peripheral B cell count	0.013	0.111	0.912
CRP	0.297	2.001	0.050

CRP, C-reactive protein.

the expression levels of CD24 and CD38 in $CD19^{hi}CD1d^{hi}$ human B cells after stimulation with CpG DNA, and our results indicated that the B cell population characterized by $CD24^{hi}CD38^{hi}$ largely overlapped with $CD19^{hi}CD1d^{hi}$ B cells (see Fig. A, Supplemental Digital Content 2, http://links.lww.com/IBD/A358). Moreover, a decreased frequency of IL-10–producing $CD24^{hi}CD38^{hi}$ B cells was found in patients with CD (see Fig. B, Supplemental Digital Content 2, http://links.lww.com/IBD/A358).

Mouse Studies

$CD19^{hi}$ and $CD1d^{hi}$ B Cells Highly Produce IL-10 in Mouse MLN Cells

Based on this result, we next investigated the expressions of CD19 and CD1d in IL-10–producing B cells isolated from mouse MLNs. Similar to the results of the human cell experiment, flow cytometry revealed that mouse B cells producing IL-10 were mainly located in the $CD19^{hi}$ and $CD1d^{hi}$ cell population (Fig. 2A). To further confirm this finding, $CD19^{hi}CD1d^{hi}$ and $CD19^{hi}CD1d^{hi}$-depleted B cells were separately sorted by flow cytometry (Fig. 2B) and their responses to CpG DNA or LPS were examined in vitro. $CD19^{hi}CD1d^{hi}$ B cells highly produced IL-10 as compared with $CD19^{hi}CD1d^{hi}$-depleted B cells after stimulation with the tested ligands, whereas the production levels of IL-6 were not different between them (Fig. 2C and D).

Adoptive Transfer of SAMP1 $CD4^+$ T Cells Induces Chronic Colitis in SCID Mice

To investigate the regulatory role of B cells producing IL-10 in intestinal inflammation, we initially established 2 types of chronic colitis models of SCID mice by adoptive transfer of whole $CD4^+$ T cells or Treg-depleted T cells ($CD4^+CD25^-$). In the colitis model cotransferred with whole B cells, reconstruction by adoptive cells was confirmed by flow cytometry (see Table, Supplemental Digital Content 3, http://links.lww.com/IBD/A359; Fig. B and D, Supplemental Digital Content 4, http://links.lww.com/IBD/A359) and immunohistochemistry (Fig. A and C, Supplemental Digital Content 4, http://links.lww.com/IBD/A360), which support the results of similar experiments recently reported.[26] Changes in several inflammatory parameters in each experimental group are shown in Figure 3. Adoptive transfers of whole and Treg-depleted T cells isolated from MLNs of SAMP1 mice induced remarkable intestinal inflammation, whereas those changes were not found in mice after transfer of $CD19^+$ B cells. In particular, the inflammatory parameters BW loss (Fig. 3A), anal colon shortening (Fig. 3C), and histological scores for the small and large intestines (Fig. 3D and E) in colitis mice after transfer of Treg-depleted T cells were more severe as compared with those in colitis mice after transfer of whole $CD4^+$ T cells.

Cotransfer with $CD19^{hi}CD1d^{hi}$-depleted B Cells Induces Severe Colitis

We also investigated the regulatory role of $CD19^{hi}CD1d^{hi}$ B cells in intestinal inflammation. Flow cytometry sorted whole or $CD19^{hi}CD1d^{hi}$-depleted B cells were intravenously injected into the present colitis models after transfer of whole $CD4^+$ T cells from SAMP1 mice, and then changes in several inflammatory parameters were evaluated. Inflammatory parameters including BW loss (Fig. 4A) and histological scores of intestines (Fig. 4B and C) in colitis mice after cotransfer of $CD19^{hi}CD1d^{hi}$-depleted B cells were more severe as compared with those in colitis mice after cotransfer of whole $CD19^+$ B cells or PBS control. In addition, expression levels of inflammatory cytokines were significantly higher in the intestinal mucosa and MLNs in colitis mice after cotransfer of $CD19^{hi}CD1d^{hi}$-depleted B cells (Fig. 4D). Because the transferred $CD19^{hi}CD1d^{hi}$ B cells freshly isolated from the MLNs of recipient mice produced significant amounts of IL-10 (see Fig. D and E, Supplemental Digital Content 4, http://links.lww.com/IBD/A360), colitis exacerbation might be dependent on depletion of $CD19^{hi}CD1d^{hi}$ B cells.

$CD19^{hi}CD1d^{hi}$ B Cells Ameliorate Intestinal Inflammation in Colitis Mice after Adoptive Transfer of Treg-depleted T Cells

We further investigated whether the regulatory effects of $CD19^{hi}CD1d^{hi}$ B cells in intestinal inflammation are dependent on the presence of Tregs. Flow cytometry sorted whole or $CD19^{hi}CD1d^{hi}$-depleted B cells were intravenously injected into colitis model mice after transfer of Treg-depleted T cells from SAMP1 mice, and then changes in several inflammatory parameters were evaluated. BW loss (Fig. 5A), histological scores of intestines (Fig. 5B and C), and expression levels of inflammatory cytokines (Fig. 5D) in the colitis mice after cotransfer of $CD19^{hi}CD1d^{hi}$-depleted B cells were more severe as compared with those in the colitis mice after cotransfer of whole $CD19^+$ B cells. These findings were similar to the experimental results obtained with the colitis

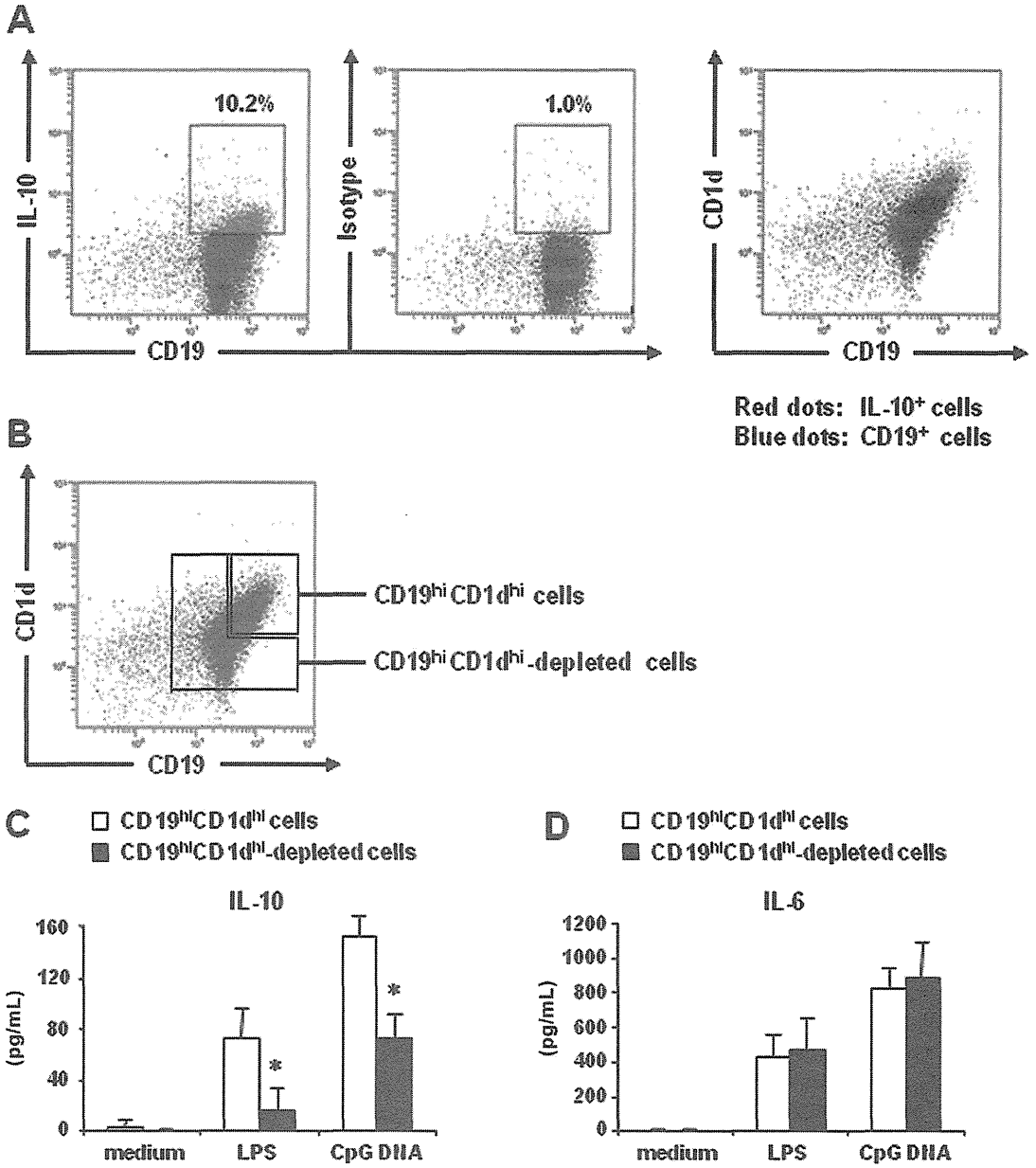

FIGURE 2. $CD19^{hi}$ and $CD1d^{hi}$ B cells highly produced IL-10 in MLN B cells of AKR mice. A, IL-10–producing B cells were detected by the presence of the cell surface markers $CD19^{hi}$ and $CD1d^{hi}$. MLN B cells isolated from 15- to 25-week-old AKR mice were incubated at 2×10^6 cells per milliliter (4×10^5 cells per well in 96-well plates) for 48 hours in medium with CpG DNA (10 nM) and stained with IL-10, CD19, and CD1d. Representative dot plots showing $IL\text{-}10^+$ cells (red dots) and whole B cells (blue dots) are presented. B, $CD19^{hi}CD1d^{hi}$ B cells highly produced IL-10, but not IL-6 after stimulation with LPS (1 μg/mL) or CpG DNA (10 nM). MLN B cells were isolated from 15- to 25-week-old AKR mice. $CD19^{hi}CD1d^{hi}$ or $CD19^{hi}CD1d^{hi}$-depleted B cells were separately sorted by flow cytometry and cultured at 2×10^6 cells per milliliter for 48 hours with LPS (1 μg/mL) or CpG DNA (10 nM). The contents of (C) IL-10 and (D) IL-6 in the culture supernatants were measured by EIA. Error bars indicate SEM values obtained from 3 independent experiments (*$P < 0.01$ versus $CD19^{hi}CD1d^{hi}$ B cells).

models after transfer of whole $CD4^+$ T cells from SAMP1 mice (Fig. 4). Since the transferred $CD4^+CD25^-$ ($Foxp3^-$) T cells may differentiate into $Foxp3^+$ Tregs during the course of colitis development in a Treg-depleted model, we performed immunostaining technique for the detection of $Foxp3^+$ cells in colonic histological sections. As shown in Figure 6 (upper panels), $Foxp3^+$ clearly infiltrated the lamina propria in the whole $CD4^+$ T cell transfer model regardless of the presence or absence of $CD19^{hi}CD1d^{hi}$ B cells. In contrast, few $Foxp3^+$ cells were detected in those sections from the Treg-depleted model (Fig. 6, lower panels).

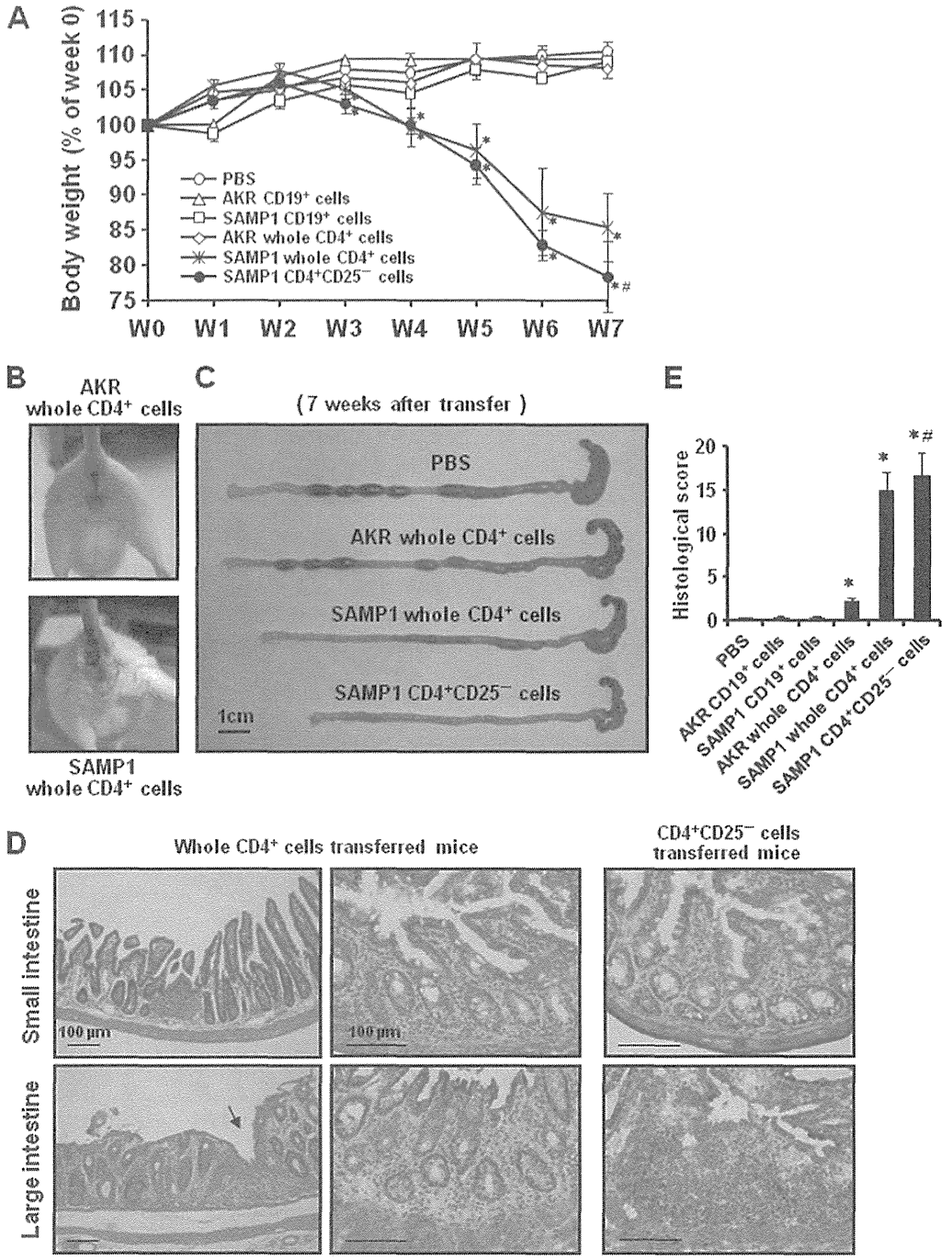

FIGURE 3. Adoptive transfer of SAMP1 $CD4^+$ T cells induced chronic colitis in SCID mice. Purified whole $CD4^+$ T cells or Treg ($CD4^+CD25^+$)-depleted T cells derived from MLN cells of SAMP1 mice were injected intraperitoneally into 8- to 10-week-old SCID mice. As a control, purified whole $CD4^+$ T cells or $CD19^+$ B cells derived from MLN cells of SAMP1 or AKR mice were injected intraperitoneally or intravenously into SCID mice. A, BW changes in experimental mice. Data are expressed as serial changes in the percentage of weight change over a 7-week period. Error bars indicate SEM values obtained from mice in each group (n = 6) ($^*P < 0.01$ versus PBS group, $^\#P < 0.01$ versus SAMP1 whole $CD4^+$ T cells group). B, Representative images of anuses of SCID mice transferred with AKR (upper) or SAMP1 (lower) MLN $CD4^+$ T cells. Anal erosions were observed in mice transferred with SAMP1 $CD4^+$ T cells. C, Representative images of colons dissected from mice in each experimental group. D, Representative images of histological changes in the small and large intestines in mice transferred with whole $CD4^+$ T cells or Treg ($CD4^+CD25^+$)-depleted T cells derived from MLN cells of SAMP1 mice. E, Mean values of intestinal histological scores in each experimental group. Error bars indicate SEM values obtained from 6 mice per group ($^*P < 0.01$ versus PBS group, $^\#P < 0.01$ versus SAMP1 whole $CD4^+$ T cells group).

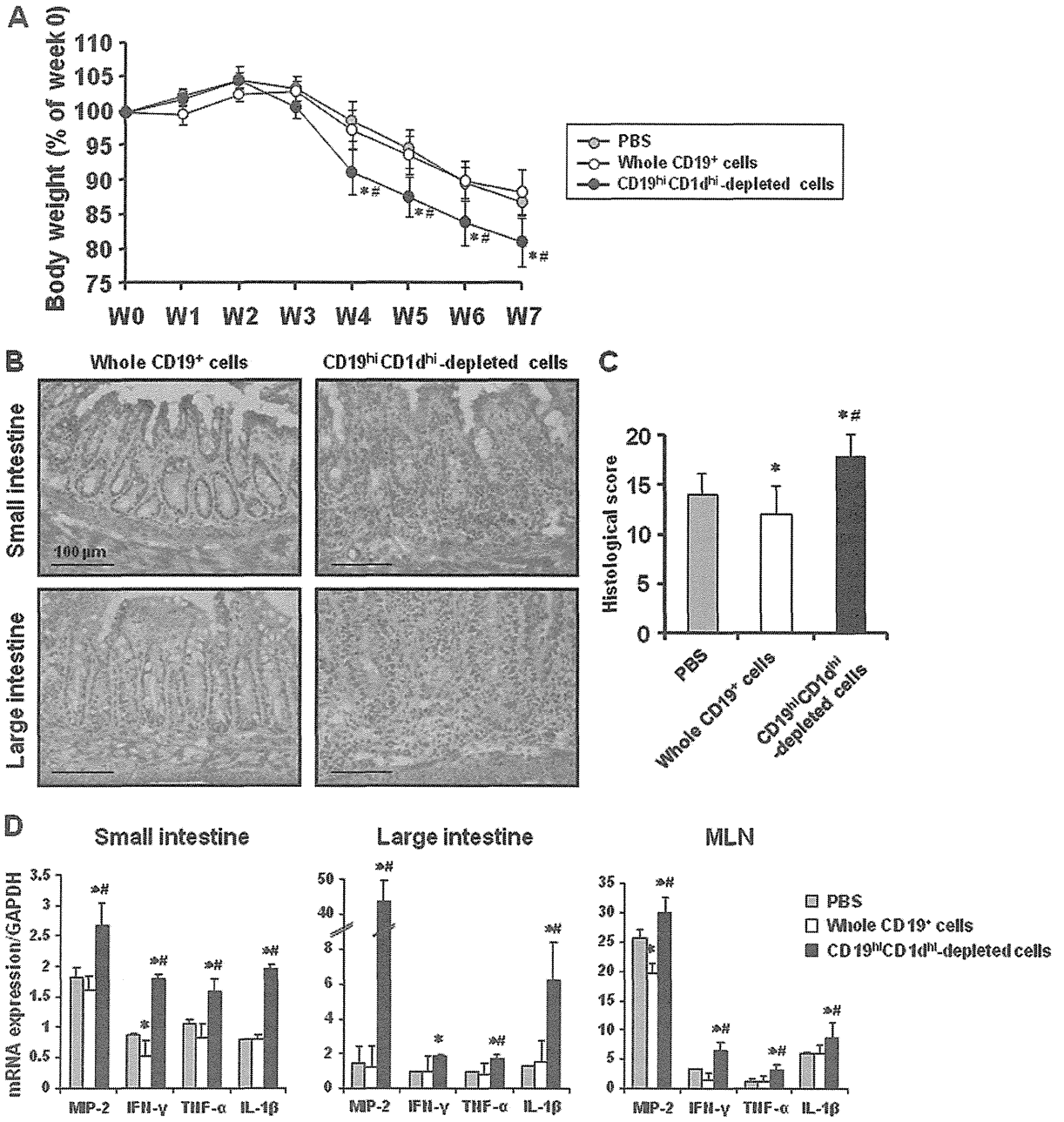

FIGURE 4. Cotransfer with CD19^{hi}CD1d^{hi}-depleted B cells induced severe colitis. Flow cytometry sorted whole or CD19^{hi}CD1d^{hi}-depleted B cells (2×10^6 cells per mouse) were intravenously injected into colitis models transferred with CD4$^+$ T cells of SAMP1 mice. A, BW changes in experimental mice. Data are expressed as serial changes in the percentage of weight change during the 7-week experimental period. Error bars indicate SEM values obtained from 9 mice per group (*$P < 0.01$ versus PBS group, $^{\#}P < 0.01$ versus whole CD19$^+$ cells group). B, Representative images of histological changes in the small and large intestines in mice with SAMP1 CD4$^+$ T cell-induced colitis cotransferred with whole or CD19^{hi}CD1d^{hi}-depleted B cells. C, Mean values of intestinal histological scores in each experimental group. Error bars indicate SEM values obtained from 9 mice per group (*$P < 0.01$ versus PBS group, $^{\#}P < 0.01$ versus whole CD19$^+$ cells group). D, Gene expressions of MIP-2, interferon-γ, TNF-α and IL-1β in the small and large intestines, and MLNs in each experimental group. Error bars indicate SEM values obtained from 9 mice per group (*$P < 0.01$ versus PBS group, $^{\#}P < 0.01$ versus whole CD19$^+$ cells group). IFN-γ, interferon-γ.

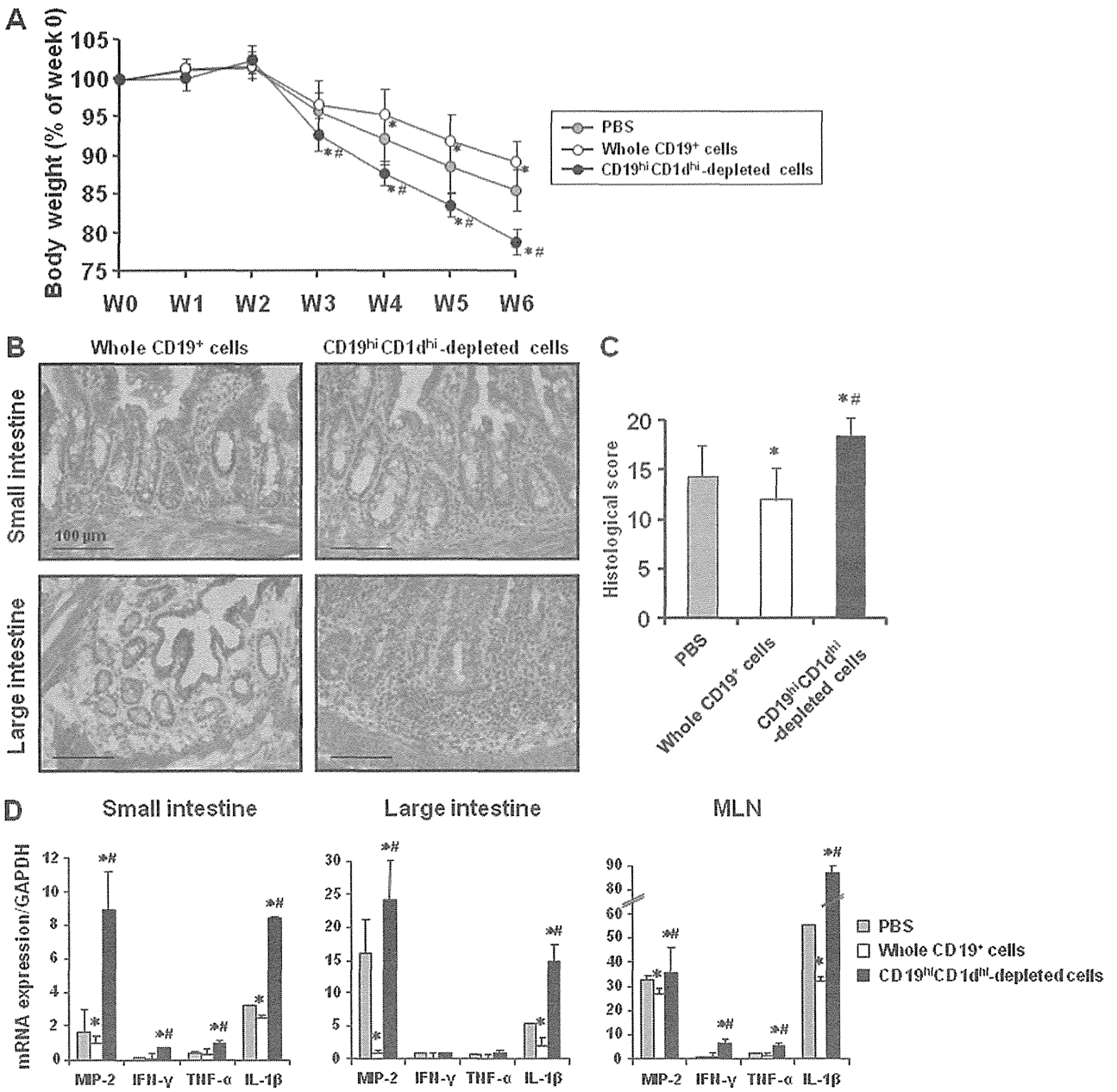

FIGURE 5. CD19^{hi}CD1d^{hi} B cells ameliorated intestinal inflammation in colitis mice by adoptive transfer of Treg-depleted T cells. Flow cytometry sorted whole or CD19^{hi}CD1d^{hi}-depleted B cells (2×10^6 cells per mouse) were intravenously injected into colitis models transferred with Treg (CD4$^+$CD25$^+$)-depleted T cells of SAMP1 mice. A, BW changes in experimental mice. Data are expressed as serial changes in percentage of weight change during the 7-week experimental period. Error bars indicate SEM values obtained from 9 mice per group ($^*P < 0.01$ versus PBS group, $^\#P < 0.01$ versus whole CD19$^+$ cells group). B, Representative images of histological changes in the small and large intestines in mice with Treg (CD4$^+$CD25$^+$)-depleted T cell-induced colitis cotransferred with whole or CD19^{hi}CD1d^{hi}-depleted B cells. C, Mean values of intestinal histological scores in each experimental group. Error bars indicate SEM values obtained from 9 mice per group ($^*P < 0.01$ versus PBS group, $^\#P < 0.01$ versus whole CD19$^+$ cells group). D, Gene expressions of MIP-2, interferon-γ, TNF-α and IL-1β in the small and large intestines, and MLNs in each experimental group. Error bars indicate SEM values obtained from 9 mice per group ($^*P < 0.01$ versus PBS group, $^\#P < 0.01$ versus whole CD19$^+$ cells group). IFN-γ, interferon-γ.

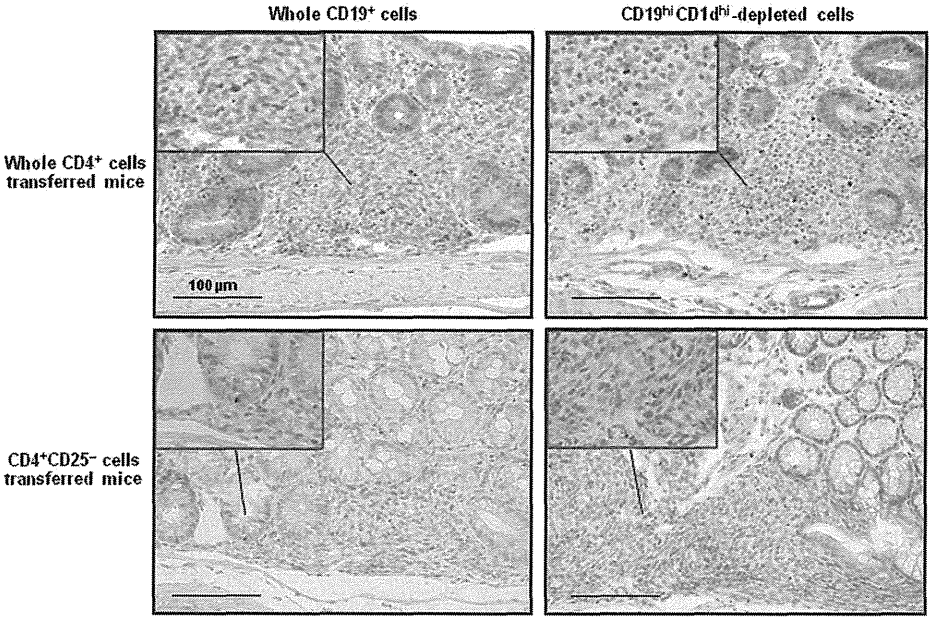

FIGURE 6. Representative immunohistochemical images of Foxp3+ cells in the lamina propria of large intestines of mice with whole $CD4^+$ or $CD4^+CD25^-$ T cell-induced colitis cotransferred with whole or $CD19^{hi}CD1d^{hi}$-depleted B cells.

These findings suggest that the anti-inflammatory function of $CD19^{hi}CD1d^{hi}$ B cells is not likely affected by Tregs.

$CD19^{hi}CD1d^{hi}$ B Cells Downregulate Cytokine Production by T Cells

CD3-stimulated $CD4^+CD25^-$ T cells were cocultured with whole $CD19^+$ B cells or Breg-depleted $CD19^+$ B cells under a CpG DNA-stimulated condition. The results of our coculture experiments indicated that the absence of $CD19^{hi}CD1d^{hi}$ B cells significantly increased CD3-induced production of TNF-α by $CD4^+CD25^-$ T cells. In addition, treatment with the anti–IL-10 antibody increased cytokine production by T cells cocultured with whole B cells (Fig. 7).

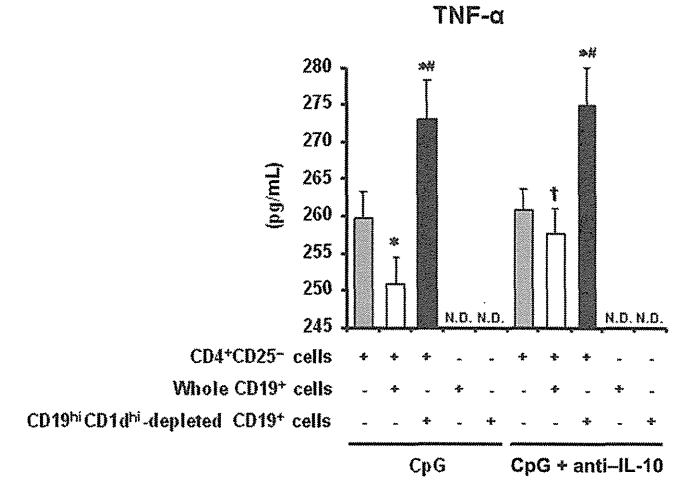

FIGURE 7. Anti-inflammatory effects of Bregs associated with IL-10 in vitro. $CD4^+CD25^-$ T cells were magnetically isolated from MLNs of SCID mice transferred with SAMP1 $CD4^+$ T cells (21 days after transfer). Whole $CD19^+$ B cells or Breg-depleted $CD19^+$ B cells were isolated from MLNs of AKR mice by flow cytometry sorting. $CD4^+CD25^-$ T cells (2×10^5 cells per well) were cocultured with whole $CD19^+$ B cells or Breg-depleted $CD19^+$ B cells (2×10^5 cells per well) in anti–CD3-coated 96-well plates with CpG DNA (10 nM) in the presence or absence of the anti–IL-10 antibody (10 μg/mL). The supernatants were analyzed by EIA for detection of various cytokine contents. Error bars indicate SEM values obtained from 4 mice per group ($^*P < 0.01$ versus PBS group, $^\#P < 0.01$ versus whole $CD19^+$ cells group, $^\dagger P < 0.01$ versus coculture of $CD4^+CD25^-$ cells and whole $CD19^+$ cells with CpG DNA group).

DISCUSSION

The present findings revealed that the level of IL-10 in CpG DNA-stimulated peripheral blood B cells was decreased in patients with CD. In addition, they also demonstrated that a lack of IL-10–producing $CD19^{hi}CD1d^{hi}$ B cells exacerbated intestinal inflammation in adaptive transfer colitis model mice regardless of the presence or absence of Tregs. These novel findings show the regulatory role of $CD19^{hi}CD1d^{hi}$ B cells in intestinal inflammation and suggest that the function of Bregs may be related to the pathogenesis of CD.

Dysfunction of Bregs has been reported to influence the pathogenesis of a variety of immune-mediated disorders, including multiple sclerosis,[27,28] systemic lupus erythematosus,[12,13,18,29] rheumatoid arthritis,[10,19] allergic airway inflammation,[16] contact hypersensitivity,[30] and experimental autoimmune encephalomyelitis.[8,17,31,32] These results were provided by experiments with

murine experimental models and human studies. In addition to autoimmune and allergic diseases, intestinal inflammation is also regulated by the functions of Bregs, which has been confirmed by several studies that used murine colitis models generated by gene targeting of T cell receptor-α,[6] G protein αi2 subunit,[11,33] or p110δ phosphoinositide 3-kinase.[34] We recently reported that CpG DNA-induced IL-10 production in intestinal B cells was decreased in SAMP1 mice.[23] Although the regulatory functions of B cells in intestinal inflammation have been demonstrated using experimental colitis models, there are few reports regarding the role of Bregs in the pathogenesis of human IBD.

In this study, we investigated IL-10 production in peripheral blood B cells obtained from patients with IBD and healthy controls. Our results revealed that the production level of IL-10 in B cells was decreased in patients with CD under basal and CpG DNA-stimulated conditions, as compared with those in patients with UC and healthy controls, which was further confirmed by multiple regression analysis that evaluated the various clinical backgrounds of the subjects. This is the first known study to suggest that Bregs dysfunction is associated with the pathogenesis of CD.

A variety of cell surface molecules, such as CD1d, CD5, CD19, CD21, CD23, CD24, CD27, CD38, Tim-1, IgM, and IgD have been used for detecting Bregs by evaluating their expression levels and coexpression patterns in IL-10–producing B cells.[9,12,15,18,28,30,31,35–39] Possible cell surface markers have mainly been identified by studies using mice disease models. For example, Tedder et al demonstrated that a subset of B cells, termed "B10 cells", expressing $CD19^{hi}CD1d^{hi}CD5^{+}$ had regulatory functions by producing IL-10.[30,31] The regulatory functions of B10 cells were first defined in a contact hypersensitivity mouse model of T cell-mediated inflammation.[30] In this study, we focused on CD19 and CD1d as possible markers of Bregs and investigated their expression levels in IL-10–producing intestinal B cells from AKR mice. Our results revealed that cells producing IL-10 were enriched in a population of B cells expressing $CD19^{hi}CD1d^{hi}$ under a CpG DNA-stimulated condition. In addition, we also examined the expressions of CD19 and CD1d in human peripheral blood samples and found the enrichment of IL-10–producing B cells in a cell population expressing $CD19^{hi}CD1d^{hi}$. This is a novel finding and useful for the detection of a human regulatory subset of B cells. Although IL-10 expression was mainly detected in $CD19^{hi}CD1d^{hi}$ B cells in the human samples, it was also found in a small population of $CD19^{low\text{-}mid}CD1d^{hi}$ B cells. In this regard, human Bregs producing IL-10 were not completely defined by $CD19^{hi}$ and $CD1d^{hi}$. Recently, Blair et al reported that $CD19^{+}CD24^{hi}CD38^{hi}$ B cells exhibited a regulatory capacity in human healthy individuals, whereas they were functionally impaired in patients with systemic lupus erythematosus.[18] In this study, we also found that the B cell population characterized by $CD24^{hi}CD38^{hi}$ was largely overlapped with $CD19^{hi}CD1d^{hi}$ B cells. Thus, the cell surface markers of human Bregs have yet to be been fully confirmed. Identification of appropriate markers is necessary to further elucidate the role of Bregs in human immune-mediated diseases.

Regulatory roles of B cells in several colitis models such as TCR-α- or Gαi2-deficient mice have been previously reported.[6,11,33] However, the precise function of $CD19^{hi}CD1d^{hi}$ B cells in intestinal inflammation remains unknown. Recently, Yanaba et al reported that dextran sulfate sodium-induced colonic injury was exacerbated in CD19-deficient mice, which was attenuated by adaptive transfer of B10 cells ($CD1d^{hi}CD5^{+}$) derived from wild-type mice.[40] The present findings revealed a regulatory role of B cells in acute intestinal injury. Because CD is a chronic intestinal immune disorder, results of experiments using a chronic colitis model are more reliable to confirm the role of Bregs in the pathogenesis of CD. Thus, we established a chronic colitis model using SCID mice by adoptive transfer of $CD4^{+}$ T cells derived from MLNs of SAMP1 mice. Because adaptive transfer of $CD4^{+}$ T cells induced conspicuously chronic inflammation in the small and large intestines, we used this model to investigate the role of Bregs in intestinal inflammation by cotransfer with whole or $CD19^{hi}CD1d^{hi}$-depleted B cells. Our results indicated that the inflammatory activity was significantly greater in colitis model mice after cotransfer of $CD19^{hi}CD1d^{hi}$-depleted B cells as compared with that in colitis mice after cotransfer of whole $CD19^{+}$ B cells or PBS control. Thus, Bregs contribute for maintaining immune regulation and protecting exacerbation of chronic intestinal inflammation.

Several studies of the association of $CD4^{+}CD25^{+}$ Tregs in Breg-mediated immunoregulation have been presented.[11,16,29] Amu et al[16] reported that Bregs prevented and reversed allergic airway inflammation by inducing Tregs in a mouse model. However, Matsushita et al[17] reported that Bregs (B10 cells) and Tregs have independent roles for controlling the initiation and late-phase immunopathogenesis of experimental autoimmune encephalomyelitis. Olson et al previously revealed that SAMP1 B cells blocked the function of Tregs and exacerbated ileitis in an SCID mouse model transferred with $CD4^{+}$ T cells.[41] However, they did not comment regarding the role of Bregs in the pathogenesis of this model. In this study, we investigated whether the role of $CD19^{hi}CD1d^{hi}$ B cells is dependent on the presence of Tregs in a mouse adaptive transfer colitis model and found that those cells attenuated intestinal inflammation in a Treg-depleted condition. Because few $Foxp3^{+}$ cells were detected in the lamina propria of the Treg-depleted model, Tregs may be less likely to contribute to the anti-inflammatory function of Bregs during colitis. Apart from conventional $CD4^{+}CD25^{+}$ Tregs, Wei et al[11] showed that B cell-mediated immunoregulation in mice colitis models requires a regulatory $CD4^{+}CD8\alpha^{+}$ T cell population. Thus, it remains unclear whether or how the functions of Bregs are dependent on Tregs. Since several novel subsets of Tregs have been recently discovered, those should be examined to further elucidate the functions of Bregs.

We also performed several in vitro experiments to evaluate the anti-inflammatory role of $CD19^{hi}CD1d^{hi}$ B cells in association with IL-10 production. Results of coculture experiments demonstrated that the absence of $CD19^{hi}CD1d^{hi}$ B cells increased cytokine production by T cells. Furthermore, cytokine production by T cells cocultured with whole B cells was partially dependent on the function of IL-10. These findings suggest that Bregs